ISSN (Print) 1226-1750
ISSN (Online) 2233-6656
Journal of Magnetics 26(3), 347-355 (2021) https://doi.org/10.4283/JMAG.2021.26.3.347

Characteristics of Modified Diffusion Analysis of Squeezed Hydro-magnetic Nanofluid Flow

S. Ahmad[1]*, Samreen Sheriff[3], and M. Farooq[2]

[1]*Department of Mathematics and Statistics, Riphah International University, Islamabad 44000, Pakistan*
[2]*Department of Pure and Applied Mathematics, The University of Haripur, Haripur, KPK, Pakistan*
[3]*DBS&H, CEME, National University of Sciences and Technology, Islamabad 44000, Pakistan*

(Received 23 March 2021, Received in final form 10 September 2021, Accepted 13 September 2021)

This communication based on nanofluid theory is exhibited to study the squeezing mechanism. Hydro-magnetic phenomenon is incorporated in the analysis of nanofluid flow. The flow of heat and mass transport is interpreted by the constitutive relationship of modified diffusion model which overcomes the deficiencies in Fourier's and Fick's classical theories. The nano-fluid theory also incorporates the features of two important slip mechanisms namely Brownian diffusion and thermophoresis. Resulting heat and mass transport problems are figure out to develop the series solutions. Interval of convergence is established for computed series solutions. Behavior of emerging parameters in flow distributions are graphed and discussed. The major founds in this attempt is that higher Brownian diffusion strengthens the both heat and mass fluxes, while larger thermophoresis parameter enhances the heat flux but it weakens the mass flux. Moreover, both heat and mass flow field decays for enlarge estimation of thermal and solutal time relaxation parameters, respectively. Velocity field shows dual behavior for dominant magnetic parameter.

Keywords : squeezing flow, nanofluid, Magneto-hydrodynamics (MHD), brownian motion, thermophoresis diffusion, modified double diffusive model

1. Introduction

Understanding the novel flow behavior of rheological fluid material (i.e. nano-fluids) are appealing research area for scientists and engineers which is even not able to explore it completely. Thus, nano-size particles are blend in base fluid forming a new class of fluid material named as nanofluid. Thus, Nanofluid is valuable to enhance the characteristics of thermal conductivity than the pure liquids having low intensity of thermal conductivity which seriously affect the heat transfer rate. Hence thermal features of conventional base fluid are achieved in perspective of nano-fluid. Innovative behavior of nano-fluid makes them significant in designing and advanced processes associated with microelectronics, food processing, fuel cells, biomedicine, hybrid-powered engines etc. In this regard, Choi [1] presented the work on nano-fluids initially. Buongiorno [2] disclosed the convective transportation of nano-fluids. Features of squeezed magneto-hydrodynamic nano-liquid flow are exposed by Sobamowo and Akinshil [3]. Kandasamy *et al.* [4] discussed the behavior of nanoparticles in hydro magneto flow of squeezed nanomaterial through porous surface. Flow behavior of heat and mass transport on squeezed Casson nano-liquid with magnetic effects is portrayed by Rashidi *et al.* [5]. Gorji *et al.* [6] described the features of heat transport in squeezed magneto-hydrodynamics nano-fluid flow. Influence of thermal radiation in heat transfer flow of squeeze MHD nanofluid is depicted by Dogonchi *et al.* [7]. Atlas *et al.* [8] illustrated the radiative squeezing flow of nano-fluid through parallel surfaces. Mahanthesh *et al.* [9] exposed the chemically reactive nano-fluid flow through exponentially shrinking sheet with partial slip. Some recent interesting investigations regarding nanofluid are presented in [10-12].

Transportation features in heat and mass exchange ensure when temperature and concentration differences happen naturally. Thus, mechanism of transportation of heat and mass is explained through Fourier's and Fick's theories in last few decades. However, in 1948 Cattaneo

*Corresponding author: Tel: +923335377399
e-mail: shakeel_oiiui@yahoo.com

[13] constructed the idea to characterize the effectiveness of heat transport phenomenon with inclusion of thermal relaxation time. Since different flow material reflect different relaxation times. Christov [14] implied the time derivative model which termed as Cattaneo-Christov diffusion model. Bachok *et al.* [15] painted the features of heat transport in nanomaterial flow upon rotating permeable disk. Muhammad *et al.* [16] disclosed the features of modified theories of double diffusive fluxes on squeezing flow of nano-liquid. Slip flow behavior of Maxwell nanomaterial incorporates Cattaneo-Christov dual diffusive model through shrinking sheet is disclosed by Sui *et al.* [17]. Hayat *et al.* [18] exhibited the modified version of heat and mass diffusive models employed to flow of Burgers nano-fluid under boundary layer assumption. Haq *et al.* [19] portrayed the hydro-magneto (MHD) flow of convectively heated fluid over stretchable sheet with velocity slip and carbon nanotubes. Variation of modified heat and mass fluxes in Powell Eyring nano-liquid flow over stretchable plate is exposed by Upadhay *et al.* [20]. Acharya *et al.* [21] exposed the aspects of modified laws of Fourier and Fick in magneto Maxwell nano-fluid flow past an inclined stretched surface. Hayat *et al.* [22] constructed the nano-fluid flow featured via modified Fourier and Fick laws in 3-dimensional coordinate system. Javed *et al.* [23] disclosed the hydro-magneto flow of a convective Ferro-fluid filled in square cavity embedded in Darcian medium. Hayat *et al.* [24] exposed the consideration of non-Fourier heat flux on fluid flow upon variable thicked rotating disk. Few recent researches on Cattaneo-Christov include [25-27].

Above-mentioned studies reveal that few terms are missing in the analyses that were carried out via nano-fluid flow with double diffusive model of Cattaneo-Christov. Such missing terms comprise Brownian diffusion and thermophoresis with thermal and solutal relaxation time. Thus, in this perspective the current attempt is to disclose the influence of non-Fourier and Fick fluxes on the flow behavior of squeezed nano-liquid. Analytic series solutions [28-33] of the flow problem are acquired which is then utilized to examine the pertinent parameters of interest graphically. Skin friction co-efficient (drag force) is graphed and analyzed.

2. Description of Problem

A hydro magneto nano-fluid is composed of continuous distribution of nano-size particles which squeezes between two parallel plates in the frame of well-known Cattaneo-Christov heat and mass flux theory. The motion in the fluid is generated by upper plate located at $y = h(t)$ having

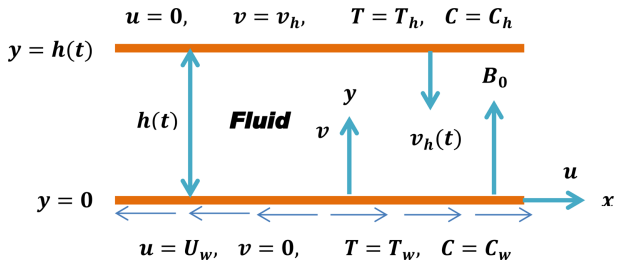

Fig. 1. (Color online) Schematic configuration of flow problem.

vertical squeezing velocity $-(\gamma/2)\sqrt{v/a(1-\gamma t)}$. Here $h(t) = \sqrt{v(1-\gamma t)/a}$ is a small distance between the plates. The lower plate at $y = 0$ is fixed and stretched in its own plane with velocity $ax/(1-\gamma t)$. We choose Cartesian coordinate system (x, y) in order to explore the flow behavior in which axes x is along the lower plate and y is along normal direction (See Fig. 1). Fundamental laws which describe the unsteady squeezed motion of an incompressible viscous nano-fluid are:

$$\frac{\partial u}{\partial x}+\frac{\partial v}{\partial y}=0, \tag{1}$$

$$\frac{\partial u}{\partial t}+u\frac{\partial u}{\partial x}+v\frac{\partial u}{\partial y}=-\frac{1}{\rho}\frac{\partial p}{\partial x}+\upsilon\left(\frac{\partial^2 u}{\partial x^2}+\frac{\partial^2 u}{\partial y^2}\right)-\frac{\sigma B_0^2}{\rho}u, \tag{2}$$

$$\frac{\partial v}{\partial t}+u\frac{\partial v}{\partial x}+v\frac{\partial v}{\partial y}=-\frac{1}{\rho}\frac{\partial p}{\partial y}+\upsilon\left(\frac{\partial^2 v}{\partial x^2}+\frac{\partial^2 v}{\partial y^2}\right), \tag{3}$$

$$(\rho C)_f\left(\frac{\partial T}{\partial t}+\boldsymbol{V}.\boldsymbol{\nabla}T\right)-(\rho C)_p\left(D_B\boldsymbol{\nabla}C.\boldsymbol{\nabla}T+\frac{D_T}{T_h}(\boldsymbol{\nabla}T)^2\right)=-\boldsymbol{\nabla}.\boldsymbol{q}, \tag{4}$$

$$\left(\frac{\partial C}{\partial t}+\boldsymbol{V}.\boldsymbol{\nabla}C\right)-\frac{D_T}{T_h}\boldsymbol{\nabla}^2T=-\boldsymbol{\nabla}.\boldsymbol{J}. \tag{5}$$

Here u and v are velocity components along x and y direction, respectively. υ represents kinematics viscosity, p represents pressure, ρ denotes the fluid density, $(\rho C)_f$ denotes heat capacity of nano-fluid, $(\rho C)_p$ represents heat capacity of nanoparticle, σ represents electric conductivity, T is fluid temperature, C is nanoparticles concentration, T_h is the upper wall temperatures, D_B represents Brownian motion co-efficient, B_0 represents applied magnetics strength, D_T represents thermophoresis co-efficient. $\tau = (\rho C)_p/(\rho C)_f$ represents the ratio between heat capacity of nano-particles to heat capacity of fluid.

Non-Fourier and non-Fick concepts are adopted which fulfill the following expression for heat flux $\boldsymbol{q}$ and mass flux $\boldsymbol{J}$ respectively.

$$\boldsymbol{q}+\delta_E\left(\frac{\partial \boldsymbol{q}}{\partial t}+\boldsymbol{V}.\boldsymbol{\nabla}\boldsymbol{q}+(\boldsymbol{\nabla}.\boldsymbol{V})\boldsymbol{q}-\boldsymbol{q}.\boldsymbol{\nabla}\boldsymbol{V}\right)=-K\boldsymbol{\nabla}T, \tag{6}$$

$$\boldsymbol{J}+\delta_C\left(\frac{\partial \boldsymbol{J}}{\partial t}+\boldsymbol{V}.\boldsymbol{\nabla}\boldsymbol{J}+(\boldsymbol{\nabla}.\boldsymbol{V})\boldsymbol{J}-\boldsymbol{J}.\boldsymbol{\nabla}\boldsymbol{V}\right)=-D_B\boldsymbol{\nabla}C, \tag{7}$$

where δ_E represents the thermal relaxation time, $\boldsymbol{V}$ denotes the velocity and δ_C represents the solutal relaxation time. Classical laws of Fourier and Fick are restored by taking $\delta_E = \delta_C = 0$ in equations (6) and (7). Equations (6) and (7) for incompressible fluid take the forms

$$\boldsymbol{q} + \delta_E \left(\frac{\partial \boldsymbol{q}}{\partial t} + \boldsymbol{V}.\boldsymbol{\nabla q} - \boldsymbol{q}.\boldsymbol{\nabla V} \right) = -K\boldsymbol{\nabla} T, \tag{8}$$

$$\boldsymbol{J} + \delta_C \left(\frac{\partial \boldsymbol{J}}{\partial t} + \boldsymbol{V}.\boldsymbol{\nabla J} - \boldsymbol{J}.\boldsymbol{\nabla V} \right) = -D_B \boldsymbol{\nabla} C, \tag{9}$$

where D_B and K denote the mass diffusivity and thermal conductivity, respectively.

On comparison from equations (8-9) to (4-5), the basic conservation laws (4) and (5) take the form as

$$\begin{aligned}
&\frac{\partial T}{\partial t} + u\frac{\partial T}{\partial x} + v\frac{\partial T}{\partial y} + \delta_E \left(\frac{\partial^2 T}{\partial t^2} + u\frac{\partial u}{\partial x}\frac{\partial T}{\partial x} + v\frac{\partial v}{\partial y}\frac{\partial T}{\partial y} + u^2\frac{\partial^2 T}{\partial x^2} \right. \\
&+ v^2\frac{\partial^2 T}{\partial y^2} + \frac{\partial u}{\partial t}\frac{\partial T}{\partial x} + 2uv\frac{\partial^2 T}{\partial x \partial y} + 2u\frac{\partial^2 T}{\partial t \partial x} + u\frac{\partial v}{\partial x}\frac{\partial T}{\partial y} + \frac{\partial v}{\partial t}\frac{\partial T}{\partial y} \\
&\left. + v\frac{\partial u}{\partial y}\frac{\partial T}{\partial x} + 2v\frac{\partial^2 T}{\partial t \partial y} \right) - \tau D_B \delta_E \left(\frac{\partial C}{\partial x}\frac{\partial^2 T}{\partial x \partial t} + \frac{\partial C}{\partial y}\frac{\partial^2 T}{\partial y \partial t} + \frac{\partial T}{\partial x}\frac{\partial^2 C}{\partial x \partial t} \right. \\
&+ \frac{\partial T}{\partial y}\frac{\partial^2 C}{\partial y \partial t} + u\frac{\partial C}{\partial x}\frac{\partial^2 T}{\partial x^2} + u\frac{\partial T}{\partial x}\frac{\partial^2 C}{\partial x^2} + u\frac{\partial C}{\partial y}\frac{\partial^2 T}{\partial x \partial y} + u\frac{\partial T}{\partial y}\frac{\partial^2 C}{\partial x \partial y} \\
&+ v\frac{\partial C}{\partial x}\frac{\partial^2 T}{\partial x \partial y} + v\frac{\partial T}{\partial x}\frac{\partial^2 C}{\partial x \partial y} + v\frac{\partial C}{\partial y}\frac{\partial^2 T}{\partial y^2} + v\frac{\partial T}{\partial y}\frac{\partial^2 C}{\partial y^2} \Big) \\
&- 2\frac{\tau D_T}{T_h}\delta_E \left(\frac{\partial T}{\partial x}\frac{\partial^2 T}{\partial x \partial t} + \frac{\partial T}{\partial y}\frac{\partial^2 T}{\partial y \partial t} + u\frac{\partial T}{\partial x}\frac{\partial^2 T}{\partial x^2} + u\frac{\partial T}{\partial y}\frac{\partial^2 T}{\partial x \partial y} \right. \\
&\left. + v\frac{\partial T}{\partial x}\frac{\partial^2 T}{\partial x \partial y} + v\frac{\partial T}{\partial y}\frac{\partial^2 T}{\partial y^2} \right) = \frac{K}{(\rho C)_f}\left(\frac{\partial^2 T}{\partial x^2} + \frac{\partial^2 T}{\partial y^2} \right) \\
&+ \tau D_B \left(\frac{\partial T}{\partial x}\frac{\partial C}{\partial x} + \frac{\partial T}{\partial y}\frac{\partial C}{\partial y} \right) + \frac{\tau D_T}{T_h}\left(\left(\frac{\partial T}{\partial x} \right)^2 + \left(\frac{\partial T}{\partial y} \right)^2 \right),
\end{aligned} \tag{10}$$

$$\begin{aligned}
&\frac{\partial C}{\partial t} + u\frac{\partial C}{\partial x} + v\frac{\partial C}{\partial y} + \delta_C \left(\frac{\partial^2 C}{\partial t^2} + u\frac{\partial u}{\partial x}\frac{\partial C}{\partial x} + v\frac{\partial v}{\partial y}\frac{\partial C}{\partial y} + u^2\frac{\partial^2 C}{\partial x^2} \right. \\
&+ v^2\frac{\partial^2 C}{\partial y^2} + \frac{\partial u}{\partial t}\frac{\partial C}{\partial x} + 2uv\frac{\partial^2 C}{\partial x \partial y} + 2u\frac{\partial^2 C}{\partial t \partial x} + u\frac{\partial v}{\partial x}\frac{\partial C}{\partial y} + \frac{\partial v}{\partial t}\frac{\partial C}{\partial y} \\
&\left. + v\frac{\partial u}{\partial y}\frac{\partial C}{\partial x} + 2v\frac{\partial^2 C}{\partial t \partial y} \right) - \frac{D_T}{T_h}\delta_C \left(\frac{\partial^3 T}{\partial x^2 \partial t} + \frac{\partial^3 T}{\partial y^2 \partial t} + u\frac{\partial^3 T}{\partial x^3} \right. \\
&\left. + u\frac{\partial^3 T}{\partial x \partial y^2} + v\frac{\partial^3 T}{\partial x^2 \partial y} + v\frac{\partial^3 T}{\partial y^3} \right) = D_B \left(\frac{\partial^2 C}{\partial x^2} + \frac{\partial^2 C}{\partial y^2} \right) \\
&+ \frac{D_T}{T_h}\left(\frac{\partial^2 T}{\partial x^2} + \frac{\partial^2 T}{\partial y^2} \right),
\end{aligned} \tag{11}$$

with boundary conditions stated as

$$\begin{aligned}
&u = U_w = \frac{ax}{1-\gamma t},\ v = 0,\ T = T_w,\ C = C_w \quad at \quad y = 0, \\
&u = 0,\ v = v_h = \frac{dh}{dt} = -\frac{\gamma}{2}\sqrt{\frac{\upsilon}{a(1-\gamma t)}},\ T = T_h,\ C = C_h \\
&\qquad\qquad at\ \ y = h(t).
\end{aligned} \tag{12}$$

Eliminating pressure term from equations (2)-(3) and dimensionless variables are now introduced as

$$\eta = \frac{y}{h(t)},\ \Psi = \sqrt{\frac{a\upsilon}{1-\gamma t}}\, x\, f(\eta),\ u = U_w f'(\eta),$$

$$v = -\sqrt{\frac{a\upsilon}{1-\gamma t}} f(\eta),\ \theta(\eta) = \frac{T - T_h}{T_w - T_h},\ \phi(\eta) = \frac{C - C_h}{C_w - C_h}, \tag{13}$$

Condition of incompressibility condition (1) is automatically satisfied while above governing flow equations take the form as

$$f^{(iv)} + f\, f''' - f' f'' - \frac{Sq}{2}(3f'' + \eta f''') - M^2 f'' = 0, \tag{14}$$

$$\begin{aligned}
&\theta'' + Pr\left(f\theta' - \frac{1}{2}\eta Sq\theta' \right) + Pr(Nb\theta'\phi'' + Nt(\theta')^2) \\
&+ Pr\beta_e \left(\frac{1}{2}\eta Sqf'\theta' - \frac{1}{2}\eta Sq^2\theta' - \frac{1}{4}\eta^2 Sq^2\theta'' + \eta Sqf\theta'' \right. \\
&\left. + \frac{3}{2}Sqf\theta' - ff'\theta' - f^2\theta'' \right) + Pr\beta_e Nb(Sq\theta'\phi' + \frac{1}{2}\eta Sq\phi'\theta'' \\
&+ \frac{1}{2}\eta Sq\theta'\phi'' - f\phi'\theta'' - f\theta'\phi'') + Pr\beta_e Nt(Sq(\theta')^2 \\
&+ \eta Sq\theta'\theta'' - 2f\theta'\theta'') = 0,
\end{aligned} \tag{15}$$

$$\begin{aligned}
&\phi'' + PrLe\left(f\phi' - \frac{1}{2}\eta Sq\phi' \right) + \left(\frac{Nt}{Nb} \right)\theta'' + PrLe\beta_c \left(\frac{1}{2}\eta Sqf'\phi' \right. \\
&\left. - \frac{1}{2}\eta Sq^2\phi' - \frac{1}{4}\eta^2 Sq^2\phi'' + \eta Sqf\phi'' + \frac{3}{2}Sqf\phi' - ff'\phi' - f^2\phi'' \right) \\
&+ \beta_c \left(\frac{Nt}{Nb} \right)\left(Sq\theta'' + \frac{1}{2}\eta Sq\theta''' - f\theta''' \right) = 0,
\end{aligned} \tag{16}$$

with subjected boundary conditions

$$\begin{aligned}
&f(0) = 0, \quad f(1) = \frac{Sq}{2}, \quad f'(0) = 1, \quad f'(1) = 0, \\
&\theta(0) = 1, \quad \theta(1) = 0, \quad \phi(0) = 1, \quad \phi(1) = 0,
\end{aligned} \tag{17}$$

where Brownian diffusive parameter Nb, Squeezing parameter Sq, Prandtl number Pr, Solutal relaxation time parameter β_c, Thermal relaxation time parameter β_e, Magnetic parameter M, Thermophresis parameter Nt, Lewis number Le are given by

$$\begin{aligned}
&Sq = \frac{\gamma}{a},\ Nb = \frac{\tau D_B (C_w - C_h)}{\upsilon},\ Pr = \frac{\upsilon}{\alpha},\ Nt = \frac{\tau D_T (T_w - T_h)}{\upsilon T_h}, \\
&Le = \frac{\alpha}{D_B},\ \beta_e = \frac{a\delta_E}{1-\gamma t},\ \beta_c = \frac{a\delta_C}{1-\gamma t},\ M^2 = \frac{\sigma B_0^2 (1-\gamma t)}{\rho a}.
\end{aligned} \tag{18}$$

It is evident that $Sq < 0$ corresponding to away movement of the plates, while $Sq > 0$ illustrates upper

wall motion towards lower wall.

Defining drag force (skin friction) as

$$C_f = \frac{\mu(\tau_{xy})\big|_{y=h(t)}}{\rho U_w^2}, \tag{19}$$

transformed express for skin friction co-efficient takes the form:

$$(R_e)^{\frac{1}{2}} C_f = f''(1). \tag{20}$$

where $R_e = U_w x/v$ is the Reynolds number.

3. Solution Analysis

Here, convergent approach is adopted to develop the series solutions of equations (14)-(16) corresponding to condition (17). Thus, process is initiated with initial approximation and linear operator's given as

$$f_0(\eta) = \frac{1}{2}(2\eta - 4\eta^2 + 3Sq\eta^2 + 2\eta^3 - 2Sq\eta^3), \tag{21}$$

$$\theta_0(\eta) = 1 - \eta, \tag{22}$$

$$\phi_0(\eta) = 1 - \eta, \tag{23}$$

$$\mathcal{L}_f = f^{(iv)}, \quad \mathcal{L}_\theta = \theta'', \quad \mathcal{L}_\phi = \phi'', \tag{24}$$

with

$$\mathcal{L}_f(C_1 + C_2\eta + C_3\eta^2 + C_4\eta^3) = 0, \ \mathcal{L}_\theta(C_5 + C_6\eta) = 0, \\ \mathcal{L}_\phi(C_7 + C_8\eta) = 0. \tag{25}$$

where $C_i (i = 1\text{-}8)$ are arbitrary constants.

The differential equations for the problem are

$$\mathcal{L}_f[f_m(\eta) - \chi_m f_{m-1}(\eta)] = \hbar_f R_m^f(\eta), \\ \mathcal{L}_\theta[\theta_m(\eta) - \chi_m \theta_{m-1}(\eta)] = \hbar_\theta R_m^\theta(\eta), \\ \mathcal{L}_\phi[\phi_m(\eta) - \chi_m \phi_{m-1}(\eta)] = \hbar_\phi R_m^\phi(\eta), \tag{26}$$

under the boundary conditions

$$f_m(0) = 0, \quad f_m(1) = 0, \quad f_m'(0) = 0, \quad f_m'(1) = 0, \\ \theta_m(0) = 0, \quad \theta_m(1) = 0, \\ \phi_m(0) = 0, \quad \phi_m(1) = 0. \tag{27}$$

Since $R_m^f(\eta)$, $R_m^\theta(\eta)$ and $R_m^\phi(\eta)$ are nonlinear operators and for embedding parameter $q = 0$ and $q = 1$, we can write

$$\check{f}(\eta;0) = f_0(\eta), \quad \check{f}(\eta;1) = f(\eta), \\ \check{\theta}(\eta;0) = \theta_0(\eta), \quad \check{\theta}(\eta;1) = \theta(\eta), \\ \check{\phi}(\eta;0) = \phi_0(\eta), \quad \check{\phi}(\eta;1) = \phi(\eta), \tag{28}$$

and with the variation of q from 0 to 1, $\check{f}(\eta;q)$, $\check{\theta}(\eta;q)$ and $\check{\phi}(\eta;q)$ vary from the initial solutions $f_0(\eta)$, $\theta_0(\eta)$ and $\phi_0(\eta)$ to the final solutions $f(\eta)$, $\theta(\eta)$ and $\phi(\eta)$ respectively. By Taylor series, we have

$$\check{f}(\eta;q) = f_0(\eta) + \sum_{m=1}^{\infty} f_m(\eta) q^m, \ f_m(\eta) = \frac{1}{m!}\frac{\partial^m \check{f}(\eta;q)}{\partial q^m}\bigg|_{q=0}, \\ \check{\theta}(\eta;p) = \theta_0(\eta) + \sum_{m=1}^{\infty} \theta_m(\eta) q^m, \ \theta_m(\eta) = \frac{1}{m!}\frac{\partial^m \check{\theta}(\eta;q)}{\partial q^m}\bigg|_{q=0}, \\ \check{\phi}(\eta;q) = \phi_0(\eta) + \sum_{m=1}^{\infty} \phi_m(\eta) q^m, \ \phi_m(\eta) = \frac{1}{m!}\frac{\partial^m \check{\phi}(\eta;q)}{\partial q^m}\bigg|_{q=0}, \tag{29}$$

We have selected parameter (auxiliary) in the way that series (29) converge at $q = 1$. Thus we have

$$\mathrm{f}(\eta) = f_0(\eta) + \sum_{m=1}^{\infty} f_m(\eta), \\ \theta(\eta) = \theta_0(\eta) + \sum_{m=1}^{\infty} \theta_m(\eta), \\ \phi(\eta) = \phi_0(\eta) + \sum_{m=1}^{\infty} \phi_m(\eta), \tag{30}$$

here f_m, θ_m and ϕ_m represent general solutions in term of special solutions (f^*_m, θ^*_m, ϕ^*_m) given by

$$f_m(\eta) = f_m^*(\eta) + C_1 + C_2\eta + C_3\eta^2 + C_4\eta^3, \\ \theta_m(\eta) = \theta_m^*(\eta) + C_5 + C_6\eta, \\ \phi_m(\eta) = \phi_m^*(\eta) + C_7 + C_8\eta. \tag{31}$$

4. Convergence Analysis

Here, expression (30) contains variables $\hbar_f$, $\hbar_\theta$ and $\hbar_\phi$

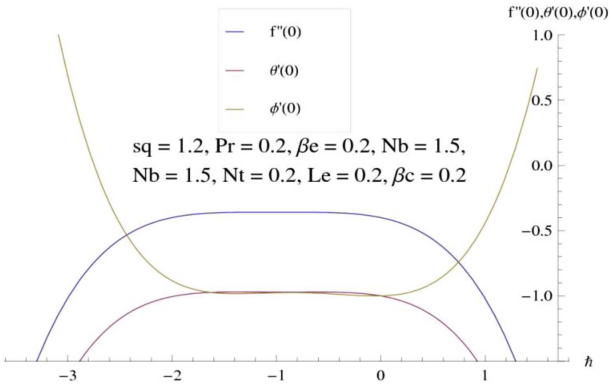

Fig. 2. (Color online) Convergence region for $f(\eta)$, $\theta(\eta)$ and $\phi(\eta)$.

which are responsible for accelerating the convergence in series solutions. Hence $\hbar$-curves for flow distributions are reflected in Fig. 2. Meaningful intervals of convergence for $f(\eta)$, $\theta(\eta)$ and $\phi(\eta)$ are [−1.8, −0.2], [−1.6, −0.2] and [−1.6, −0.2] respectively.

5. Discussion

Behavior of manifold parameters emerging in the flow problem is elaborated in this segment via graphs for velocity component, temperature and concentration fields.

5.1. Graphical illustration of velocity distribution

Figs. 3 & 4 reflect the behavior of squeezing parameter *Sq* corresponding to velocity components. Enlarge squeezing parameter causes top plate to moves closer to the bottom stretchable plate which is responsible for increment in squeezing force and consequently horizontal and vertical velocities grows. Moreover, for $Sq < 0$, the both upper and lower walls move away and for $Sq > 0$, the upper plate moves towards the lower plate, respectively, while $Sq = 0$ relative to steady case or stationary plates. Further the velocity field grows for the larger values of η. The velocity field is smaller at the lower surface while maximum at the upper plate. Fig. 5 depicts outcome of magnetic parameter *M* on velocity field. Larger magnetic parameter predicts diminishing trend of velocity in a region $0 \le \eta \le 0.5$, whereas velocity field displays opposite behavior in the region $0.5 \le \eta \le 1$. Furthermore, no variation is witnessed in the nanofluid velocity at $\eta = 0.5$. With the intensification in *M* enhances the intensity of Lorentz forces provide resists in fluid's deformation. Therefore, velocity field decays. Fig. 6 presents three dimensional graphs which show behavior of magnetic parameter (M) and squeezing parameter *Sq* on the skin friction ($(Re)^{\frac{1}{2}}C_f$). It is predicted that skin friction weakens for enlarge *Sq*, whereas it exhibits decreasing behavior throughout the material with increasing *M*. Physically, greater squeezing parameter generates more deformation in working fluid due to the squeezing force and as a consequence the C_f decays. Moreover, magnetic parameter *M* depends upon the Lorentz forces which illustrate the resistance to flow due to which the frictional force between the plate and fluid particles produces at the same rate throughout the material and as a result skin friction depicts decreasing variation throughout the material.

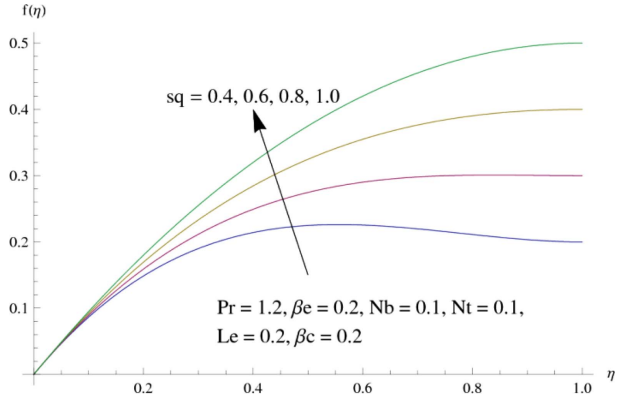

Fig. 3. (Color online) Analysis of *Sq* on $f(\eta)$.

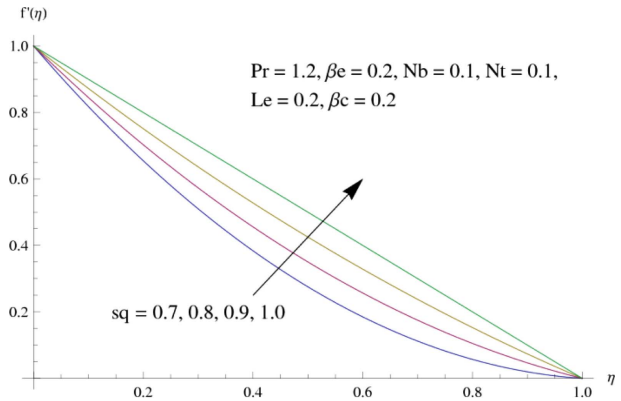

Fig. 4. (Color online) Analysis of *Sq* on $f'(\eta)$.

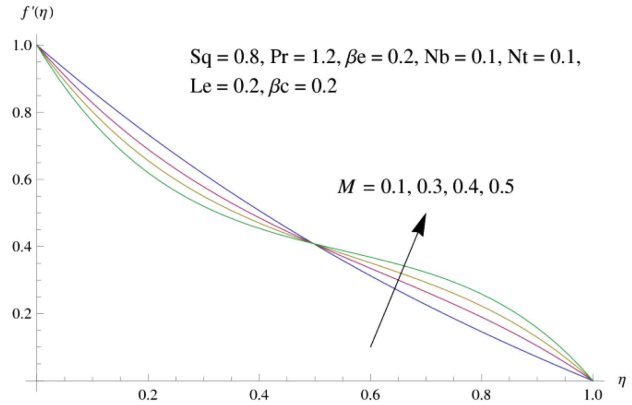

Fig. 5. (Color online) Analysis of *M* on $f'(\eta)$.

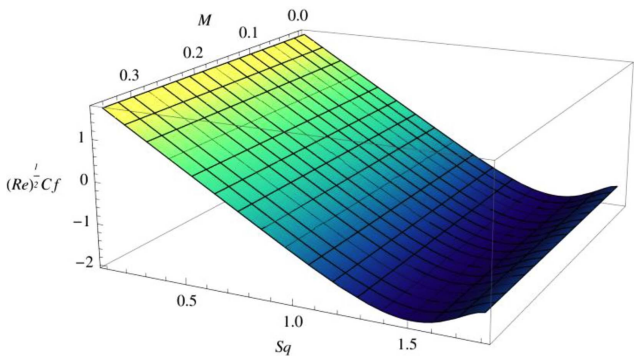

Fig. 6. (Color online) Analysis of *Sq* and *M* on C_f.

5.2. Graphical illustration of temperature distribution

Fig. 7 interprets the temperature field for different values of squeezing parameter *Sq*. Here intensify *Sq* shifts the minimum in the temperature profile. Further lower temperature exists near the upper plate. Physically more squeezing force is generated in the fluid due to dominant squeezing parameter which reduces the kinematic viscosity and consequently decline is noticed in temperature profile. Fig. 8 portrays magnetic parameter *M* outcomes on the temperature field. This figure displays the increasing behavior of temperature for larger *M*. Physically, frictional forces between nanoparticles and plate increases for dominant *M*. Therefore, temperature field grows. Fig. 9 addresses the deviation in temperature distribution when Prandtl number *Pr* varies. Fluid temperature decays because of an increment in *Pr*. Physically uplift in Prandtl number, the thermal diffusivity reduces which results in transportation of lower intensity of heat from sheet which is heated to cold liquid nearby upper wall and as a consequence liquid temperature profile weakens. Variation of temperature distribution corresponding to Brownian motion parameter *Nb* is demonstrated in Fig. 10. Temperature distribution

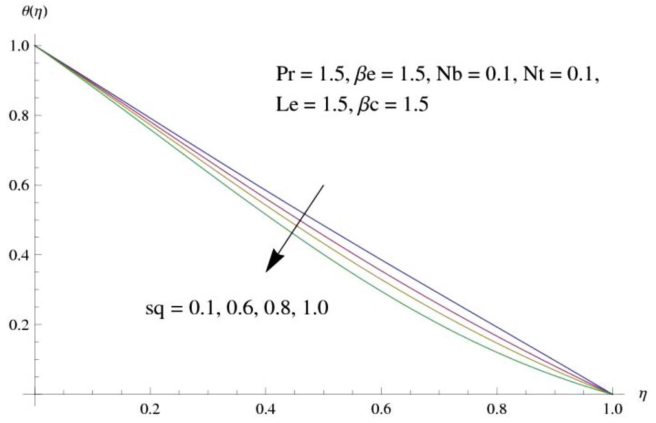

Fig. 7. (Color online) Analysis of *Sq* on $\theta(\eta)$.

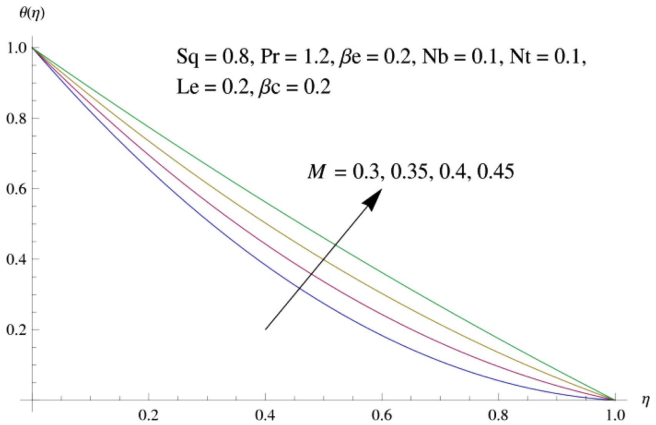

Fig. 8. (Color online) Analysis of *M* on $\theta(\eta)$.

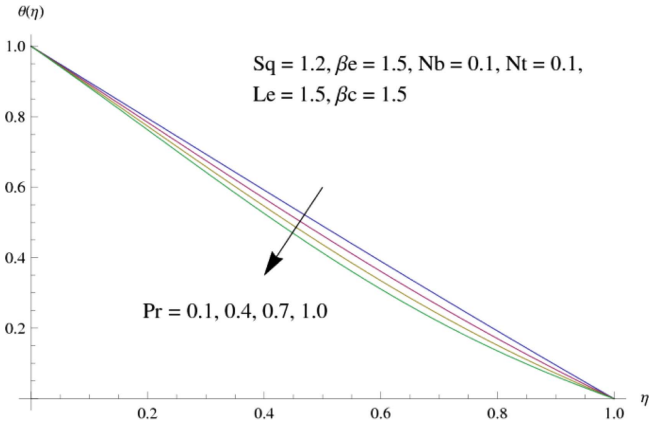

Fig. 9. (Color online) Analysis of *Pr* on $\theta(\eta)$.

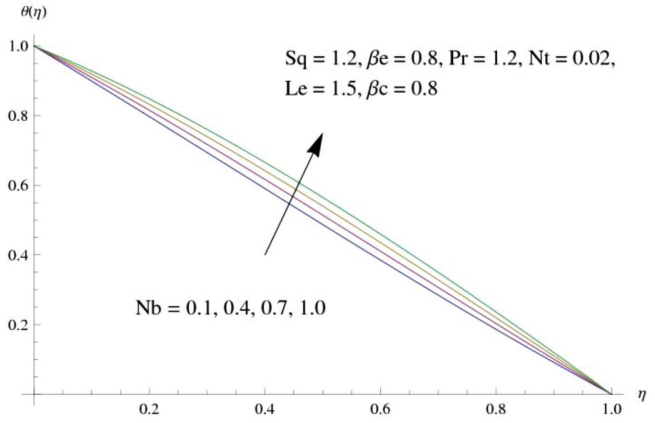

Fig. 10. (Color online) Analysis of *Nb* on $\theta(\eta)$.

strengthens for higher Brownian diffusive parameter. In fact, high intensity of Brownian diffusive parameter give rise in collisions among particles of fluid which indicates greater transport of heat from the sheet to the liquid and resultantly temperature field grows up. The variation of thermophoresis parameter *Nt* is stated in Fig. 11. Temper-

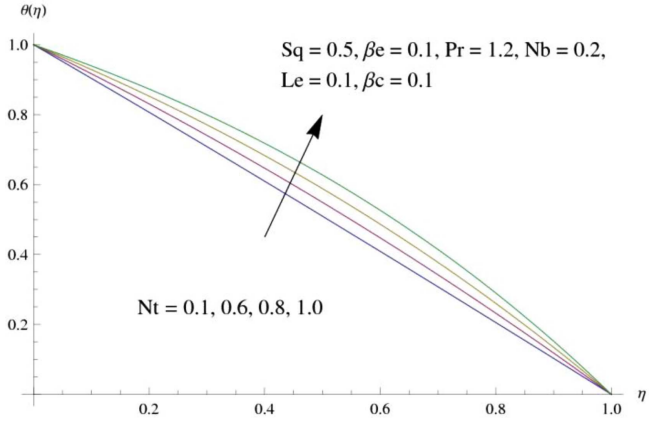

Fig. 11. (Color online) Analysis of *Nt* on $\theta(\eta)$.

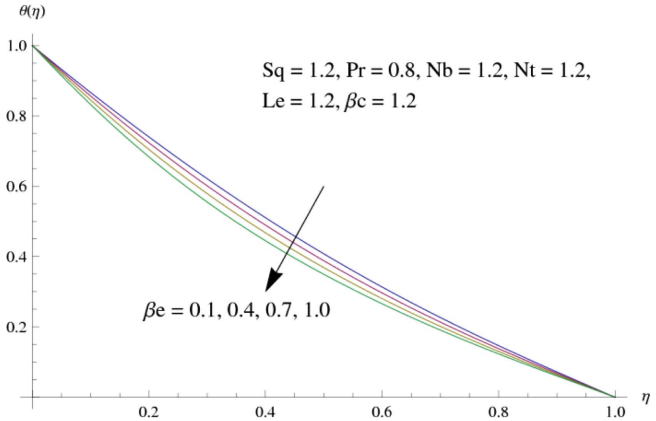

Fig. 12. (Color online) Analysis of β_e on $\theta(\eta)$.

ature field is observed to dominate corresponding to larger thermophoresis parameter. Physically for diverse values of thermophoresis parameter, the particles are taken away from sheet (heated) to fluid (cold) in the region nearby upper wall and resultantly, temperature distribution rises. Further, maximum temperature occurs near the upper plate. Fig. 12 reflects the behavior of thermal relaxation time parameter β_e on liquid temperature. It describes that temperature decays on incrementing thermal relaxation time relaxation parameter. The reason is that when we increase thermal relaxation time parameter, the fluid particles take extra time for transportation of heat to adjust particles. Resultantly temperature decreases. For $\beta_e = 0$ the heat is observed to transfer through the whole material in infinite speed and thus temperature grows for $\beta_e = 0$.

5.3. Graphical illustration of concentration distribution

The concentration distribution is graphed against squeezing parameter *Sq* in Fig. 13. Decrement is witnessed in

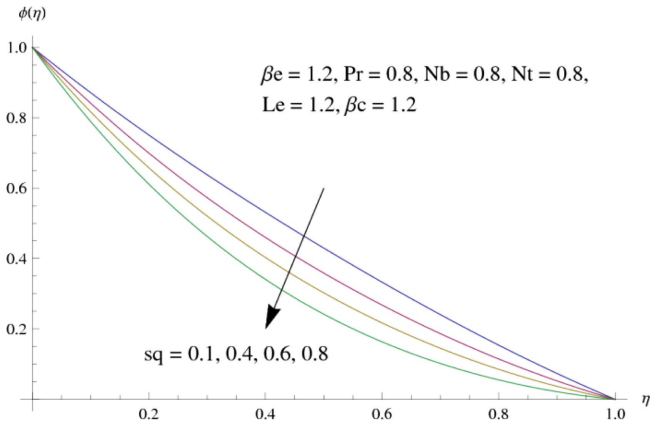

Fig. 13. (Color online) Analysis of *Sq* on $\phi(\eta)$.

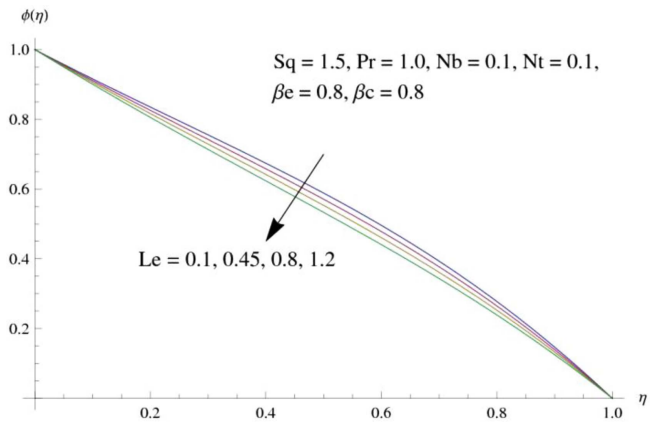

Fig. 14. (Color online) Analysis of *Le* on $\phi(\eta)$.

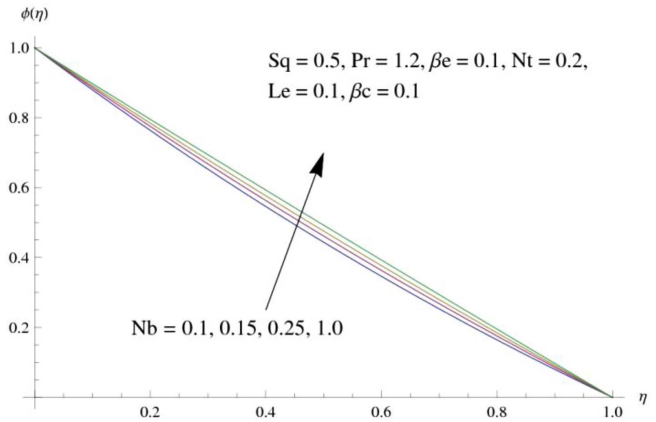

Fig. 15. (Color online) Analysis of *Nb* on $\phi(\eta)$.

concentration field for enlarge squeezing parameter. Fig. 14 discloses the features of Lewis number (*Le*) in concentration distribution. For dominant values of Lewis number result in reduction in mass diffusivity which resist fluid motion and consequently the transportation of mass from fluid to plate decays. Hence decline is noticed in

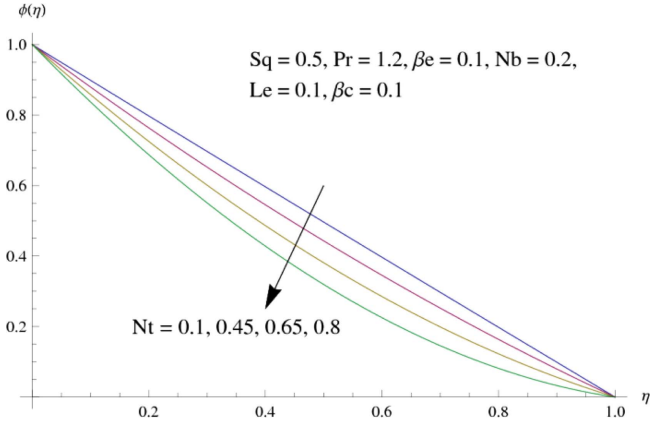

Fig. 16. (Color online) Analysis of *Nt* on $\phi(\eta)$.

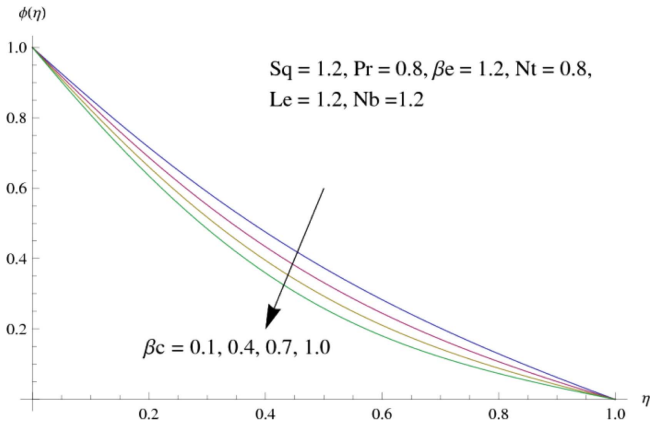

Fig. 17. (Color online) Analysis of β_c on $\phi(\eta)$.

concentration field $\phi(\eta)$. Fig. 15 shows the variation of Brownian diffusion parameter *Nb* on concentration field. By incrementing the Brownian diffusion parameter, the particles concentration increases. The reason is behind that by incrementing Brownian motion parameter molecular diffusion also dominates due to effective nanoparticles motion from top wall to the fluid. As a result due to increment in molecular diffusion, the concentration profile increases. Fig. 16 exhibits the behavior of thermophoresis parameter *Nt* on concentration field. It illustrates larger values of thermophoresis parameter leads to decay in concentration distribution. Growing thermophoresis parameter states weak force onto nanoparticles within fluid, bring about small mass diffusion. Thus, concentration distribution declines. Aspects of solutal relaxation time parameter β_c in concentration distribution are constructed in Fig. 17. With an increase in solutal relaxation time parameter concentration field reflects low intensity. In fact for dominant values of solutal relaxation time parameter, the fluid particles need extra time to penetrate which demonstrates decline in concentration field. For $\beta_c = 0$ the fluid particles instantly disperse through the whole of material. Therefore, concentration field rises for $\beta_c = 0$.

6. Closing Remarks

Cattaneo-Christov model capable of exploring the influence of heat and mass transport phenomenon on squeezed nano-fluid is addressed. Summary of performed study are listed below:

- Velocity field shows dual behavior for dominant magnetic parameter *M*.
- Temperature field is increasing function of *Nb* and *Nt*.
- Higher magnetic parameter *M* enhances the temperature field.
- Temperature field declines with a rise in thermal relaxation time parameter.
- Brownian motion parameter *Nb* strengthens the concentration field whereas thermophoresis parameter *Nt* demonstrates decrement in concentration profile.
- Enlarge solutal relaxation time parameter minimized the concentration profile.

References

[1] S. U. Choi, Proc. ASME Int. Mech. Eng. Con. Exp. **66**, 99 (1995).
[2] J. Buongiorno, J. Heat. Trans. **128**, 240 (2006).
[3] M. G. Sobamowo and A. T. Akinshilo, Alex. Eng. J. **57**, 1413 (2018).
[4] R. Kandasamy, R. Mohammad, N. A. B. M. Zailani, and N. F. B. Jaafar, J. Mol. Liq. **233**, 156 (2017).
[5] M. M. Rashidi, M. J. Babu, N. Sandeep, and M. E. Ali, J. Comp. Theo. Nano. **13**, 8700 (2016).
[6] M. R. Gorji, O. Pourmehran, M. G. Bandpy, and D. D. Ganji, J. Tai. Ins. Chem. Eng. **67**, 467 (2016).
[7] A. S. Dogonchi, K. Divsalar, and D. D. Ganji, Comp. Meth. App. Mech. Eng. **310**, 58 (2016).
[8] M. Atlas, R. U. Haq, and T. Mekkaoui, J. Mol. Liq. **223**, 289 (2016).
[9] B. Mahanthesh, F. Mabood, B. J. Gireesha, and R. S. R. Gorla, Eur. Phys. J. Plus. **132**, 113 (2017).
[10] G. Bognár, M. Klazly, and K. Hriczó, Processes **8**, 827 (2020).
[11] A. Alam, D. N. K. Marwat, and A. Ali, Adv. Mech. Eng. **13**, 1 (2021).
[12] N. Vedavathi, G. Dharmaiah, K. Venkatadri, and S. A. Gaffar, Non-lin. Eng. **10**, 159 (2021).
[13] C. Cattaneo, Mod. Reg. Emi. **3**, 83 (1948).
[14] C. I. Christov, Mech. Res. Comm. **36**, 481 (2009).
[15] N. Bachok, A. Ishak, and I. Pop, Phys. B: Con. Mat. **406**, 1767 (2011).
[16] N. Muhammad, S. Nadeem, and T. Mustafa, Res. Phys. **7**, 862 (2017).
[17] J. Sui, L. Zheng, and X. Zhang, Int. J. Therm. Sci. **104**, 461 (2016).
[18] T. Hayat, A. Aziz, T. Muhammad, and A. Alsaedi, Chin. J. Phys. **55**, 916 (2017).
[19] R. U. Haq, S. Nadeem, Z. H. Khan, and N. F. M. Noor, Phys. B: Con. Mat. **457**, 40 (2015).
[20] M. S. Upadhay, and C. S. K. Raju, Info. Med. Unlock. **9**, 76 (2017).
[21] N. Acharya, K. Das, and P. K. Kundu, Int. J. Mech. Sci. **130**, 167 (2017).
[22] T. Hayat, T. Muhammad, A. Alsaedi, and B. Ahmad, Res. Phys. **6**, 897 (2016).
[23] T. Javed, Z. Mehmood, and Z. Abbas, Phys. B: Con. Mat. **506**, 122 (2017).
[24] T. Hayat, A. Kiran, M. Imtiaz, and A. Alsaedi, Eur. Phys. J. Plus. **132**, 145 (2017).

[25] T. Muhammad, K. Rafique, M. Asma, and M. Alghamdi, Phys. A: Stat. Mech. Appl. **556**, e123968 (2020).
[26] Y. X. Li, F. Shah, M. I. Khan, R. Chinram, Y. Elmasry, and T. C. Sun, Cha. Soli. Frac. **148**, e111010 (2021).
[27] S. A. Khan, H. Waqas, S. M. R. S. Naqvi, M. Alghamdi, and Q. Al-Mdallal, Case Stud. Ther. Eng. **26**, e101017 (2021).
[28] S. J. Liao, Beyond Perturbation: Introduction to Homotopy analysis method. Boca Raton: Chapman and Hall, CRC Press (2003).
[29] S. J. Liao, Homotopy Analysis Method in Non-linear differential equations. Heidelberg: Springer and Higher Education Press (2012).
[30] T. Hayat, A. Qayyum, F. Alsaadi, M. Awais, and A. M. Dobaie, Eur. Phys. J. Plus. **128**, 85 (2013).
[31] T. Hayat, S. Ali, M. Awais, and M. S. Alhuthali, App. Math. Mech. **36**, 61 (2015).
[32] J. Zhu, D. Yang, L. Zheng, and X. Zhang, App. Math. Letter. **52**, 183 (2016).
[33] T. Hayat, A. Kiran, M. Imtiaz, and A. Alsaedi, Res. Phys. **7**, 823 (2017).